Earth and Planetary Science Letters 572 (2021) 117133

Contents lists available at ScienceDirect

Earth and Planetary Science Letters

www.elsevier.com/locate/epsl

An iron isotope perspective on back-arc basin development: Messages from Mariana Trough basalts

Yanhong Chen[a,*], Yaoling Niu[b,c,d,**], Qiqi Xue[d,e], Yajie Gao[d,f], Paterno Castillo[g]

[a] School of Ocean Sciences, China University of Geosciences, Beijing 100083, China
[b] China University of Geosciences, Beijing 100083, China
[c] Department of Earth Sciences, Durham University, Durham DH1 3LE, UK
[d] Laboratory for Marine Geology, Qingdao National Laboratory for Marine Science and Technology, Qingdao 266061, China
[e] University of Chinese Academy of Sciences, Beijing 100049, China
[f] Research School of Earth Sciences, Australian National University, Canberra ACT 2601, Australia
[g] Scripps Institution of Oceanography, University of California San Diego, 9500 Gilman Drive, La Jolla, CA 92093-0212, USA

ARTICLE INFO

Article history:
Received 26 February 2021
Received in revised form 22 July 2021
Accepted 25 July 2021
Available online 10 August 2021
Editor: R. Hickey-Vargas

Keywords:
iron isotopes
back-arc basin basalts
asthenospheric mantle
sub-arc lithospheric mantle
northern Mariana Trough

ABSTRACT

The geology and magmatism of the northern Mariana Trough (NMT) represent a type example for the development of a back-arc basin (BAB). It is a mature spreading center in the south and propagating northward via rifting of arc and rear arc lithosphere in response to trench retreat and overriding plate extension in space and time. It is thus essential to fully characterize its tectonomagmatic processes that are potentially of global significance. For this reason, we carried out a comprehensive geochemical study on basaltic samples (glasses) from the NMT axis from 17 to 23°N by analyzing a full suite of major and trace elements, Sr–Nd–Pb–Hf radiogenic isotopes and stable Fe isotopes. The Fe isotopes, in particular, have the potential to offer novel perspectives beyond the aforementioned geochemical variables. From south to north, the δ^{56}Fe of the NMT basalts (NMTB) decrease systematically, varying from a MOR-like value of +0.12‰ to an arc-like value of 0.00‰. Importantly, incompatible element abundances and Sr–Nd–Pb–Hf isotope compositions of the NMTB also show systematic along-latitude variations. Positively correlated with δ^{56}Fe, the abundances of fluid-insoluble elements (e.g., Nb, Ta, Zr, Hf, Ti and heavy rare earth elements) show the south-to-north decrease, suggesting that the NMTB δ^{56}Fe systematics are inherited from the magma source variation. The source variation is most consistent with an asthenosphere source in the south and progressively more depleted harzburgitic lithosphere source of prior melt depletion towards north. On the other hand, there are scattered but significant enrichment trends towards north in terms of Sr–Nd–Pb–Hf radiogenic isotopes and fluid-soluble incompatible elements (e.g., Ba, Rb, Cs, Th, U, K, Pb, Sr and light rare earth elements), which is consistent with south-to-north increase in slab material (e.g., slab fluids, sediments etc.) contribution. These north-to-south magma source systematics defined by the NMTB can be readily understood as a tectonic response to the back-arc basin development with time from initial arc-magmatism dominated by sub-arc lithospheric mantle melting with significant slab material contributions to back-arc rifting and to back-arc spreading center magmatism characterized by increasing asthenospheric mantle melting, decreasing slab material contribution and diminishing sub-arc lithospheric mantle participation. This tectonic-magma source evolution in space and time is manifested by the snapshot of the NMTB magmatism in terms of the geology, petrology and geochemistry.

The NMTB δ^{56}Fe values and fluid-insoluble incompatible element abundances are unaffected by slab materials, but controlled by the harzburgitic residues of previous melt extraction depleted in these elements with low δ^{56}Fe at the early arc-magmatism stage in the north and by the asthenosphere of MORB mantle characteristics in the south with well-developed back-arc spreading system. Importantly, these observations affirm the understanding that compositionally depleted and

* Corresponding author.
** Corresponding author at: China University of Geosciences, Beijing 100083, China.
E-mail addresses: chenyh@cugb.edu.cn (Y. Chen), yaoling.niu@durham.ac.uk (Y. Niu).

https://doi.org/10.1016/j.epsl.2021.117133

physically buoyant lithosphere is prerequisite as the overriding plate for subduction initiation at its edges.

1. Introduction

Back-arc basin basalts (BABB) formed at the infant back-arc rifting stage are indistinguishable from island arc basalts (IAB) that are enriched in large ion lithophile elements (LILEs) and depleted in high field strength elements (HFSEs), whereas BABB from mature back-arc spreading centers have geochemical characteristics similar to mid-ocean ridge basalts (MORB) with no or weak aforementioned IAB signature (e.g., Hawkins et al., 1990; Stern et al., 1990; Gribble et al., 1998; Pearce et al., 2005). This observation can be understood as BABB source compositional change from arc-like to MOR-like in response to the initiation and growth of back-arc spreading centers (or back-arc basins for short; BAB). We also understand that the development of BAB is a passive response to seafloor subduction, trench retreat and overriding plate extension (e.g., Niu, 2014). These geochemical and tectonic understandings altogether well explain the geochemistry (e.g., incompatible elements and Sr–Nd–Pb isotopes) of the northern Mariana Trough basalts (NMTB), i.e., basalts from the northern tip at the rifting stage are dominated by the IAB signature and change gradually into MORB-like compositions in the more mature spreading environment towards south (e.g., Stern et al., 1990; Gribble et al., 1996, 1998). This clear pattern, despite some local complexities, leads us to the hypothesis that the geology and magmatism of the NMT represent a type example of back-arc development and the associated tectonomagmatic processes may be of general and global significance. To test this hypothesis and to potentially apply this model to intra-oceanic back-arc spreading centers globally (e.g., those behind Tonga-Kermadec, Lesser Antilles, Sandwich volcanic arcs), we need to fully characterize the tectonomagmatic processes of the NMT.

For the above reason, we have carried out a comprehensive geochemical study on basaltic glasses (i.e., quenched basaltic melts) from the NMT axis from 17 to 23°N by analyzing a full suite of major and trace elements, Sr–Nd–Pb–Hf radiogenic isotopes and stable Fe isotopes. We emphasize the potential importance of Fe isotopes because Fe, as a major element, behaves differently from commonly used incompatible elements and because there is no understood reason why Fe isotopes should behave the same as radiogenic isotopes. As a result, Fe isotope compositional variation, if any, can offer a novel perspective on the NMTB petrogenesis. Importantly, despite many Fe isotope studies on mantle and mantle derived rocks (e.g., Weyer and Ionov, 2007; Williams and Bizimis, 2014), the behavior of Fe isotopes during mantle melting remains elusive, for which our recent study on seamount lavas flanking the East Pacific Rise axis is informative (Sun et al., 2020). They found that geochemically enriched lavas dominated by enriched mantle source component of low-degree melt metasomatic origin correlate with heavy Fe isotopes (i.e., high $\delta^{56,57}$Fe). This implies that mantle melting residues after heavy Fe isotope extraction are expected to have light Fe isotopes (i.e., low $\delta^{56,57}$Fe). Considering the understanding that subduction initiation is a consequence of lateral compositional buoyancy contrast within the lithosphere (Niu et al., 2003), the mantle lithosphere of the overriding plate must be harzburgitic residue of previous melt extraction that is compositionally depleted and physically buoyant relative to the subjacent asthenosphere. It follows that the NMTB source contribution is expected to change from the sub-arc lithospheric mantle dominance with limited asthenosphere participation at the northern tip to the asthenosphere dominance with diminished lithosphere participation in the more mature and better developed BAB spreading center in the south, which is also accompanied by the declining contribution of subducting slab materials. Indeed, our new data fully corroborate the above reasoning and understandings.

In the following, we present our data and discuss their significance in terms of NMT development. It is important to emphasize that (1) the correlated variations of Fe isotopes with radiogenic isotopes and incompatible element abundances do not suggest their similar or predictable geological behaviors, but do demonstrate their being consequences of our understood physical processes of BAB development and genetically related magma source material change in space and time; (2) we predict that our understanding of BAB development based on the NMT is of general significance globally to be tested in future studies.

2. Geological background and samples

The Mariana Arc is the southern segment of the ∼2500 km long Izu-Bonin-Mariana (IBM) island arc system resulting from the westward subduction of the Pacific Plate beneath the Philippine Sea Plate (Fig. 1a). The Mariana Trough is an actively spreading BAB, and is crescent-shaped located between the Mariana Arc (volcanically active arc) and the West Mariana Ridge (remnant arc; Fig. 1), with a maximum width of 250 km at about 17°N. The spreading axis is located on the eastern side of the basin, indicating highly asymmetric spreading (e.g., Deschamps and Fujiwara, 2003). Repeated GPS data surveys in the Mariana Islands indicate that the spreading rates of the Mariana Trough ranges from ∼15 mm/yr near Agrihan in the north to ∼45 mm/yr near Guam in the south (Kato et al., 2003). We focus our study on the NMT, where the extension axis changes from a mature spreading center in the south to rifting in the north (e.g., Gribble et al., 1998). The samples were collected by dredging along the NMT axis from 17 to 23°N during the 1969 SCAN (Leg 4) aboard the *R/V Argo*, the 1978 MARA (Leg 4, 6 and 7) and the 1991 TUNES (Leg 7) expeditions aboard the *R/V Thomas Washington*. Dredge locations are listed in Supplementary Table S1 and shown in Fig. 1b. Previous studies found that these rock samples show progressive changes in chemical and isotopic compositions, from BABB in the back-arc spreading center in the south to the increasingly arc-like basalts to the north, and to those indistinguishable from arc lavas towards the northernmost portion of the rift (e.g., Stern et al., 1990; Gribble et al., 1996, 1998).

3. Analytical methods

From 17 to 23°N along the NMT axis, 24 samples were selected for major and trace element analysis and isotope measurement. All the weathering surfaces and suspect contaminants of these samples were thoroughly removed. The samples were then crushed into fragments and cleaned ultrasonically before hand-picking (glasses and matrix chips) free of phenocrysts under a binocular microscope. They were further cleaned in Milli-Q water for 10 min, at least three times, in an ultrasonic bath before analysis. All the analytical work (major elements, trace elements and all the isotopes) was done in the Laboratory of Ocean Lithosphere and Mantle Dynamics in the Institute of Oceanology, Chinese Academy of Sciences.

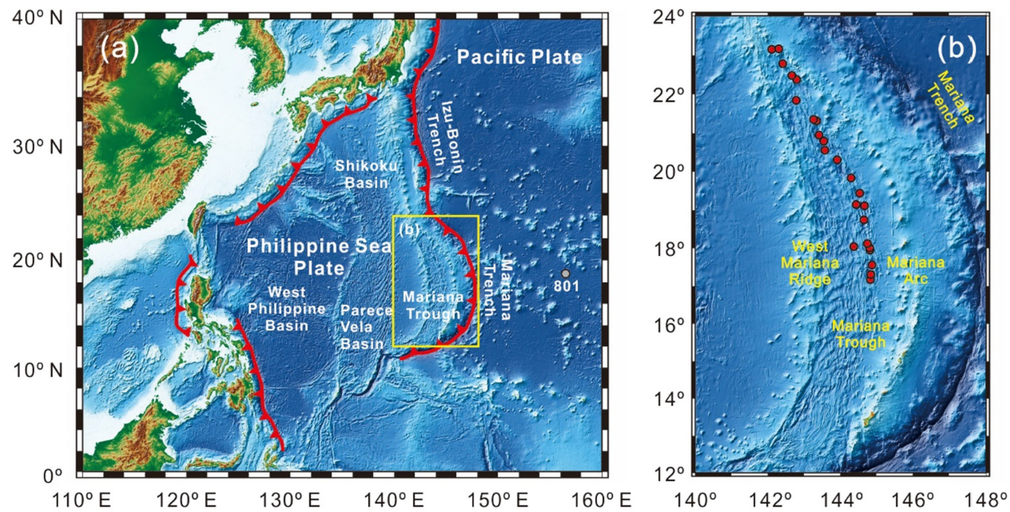

Fig. 1. Bathymetric map of the Mariana Trough showing sample locations (along northern Mariana Trough). The map is made using Generic Mapping Tools (GMT, Wessel et al., 2019).

3.1. Bulk rock Fe isotope and other isotope analyses

For Fe isotope analysis, about 5–10 mg of samples were dissolved in a distilled HNO_3-HCl-HF mixture on a hotplate at 120 °C for 15 h, and then re-dissolved, after evaporation, with distilled 3N HNO_3 for 2 h until complete dissolution. Fe was purified with a polypropylene column filled with 1 ml AG-MP-1 M resin (200–400 mesh) in a 9N HCl medium following the procedure of Gong et al. (2020). Fe was collected using 1.5 ml 1N HCl. The purified solutions were doped with GSB Ni standard (an ultrapure single elemental standard solution from the China Iron and Steel Research Institute) as an internal mass bias monitor with Ni: Fe ratio of ∼1.4:1 (Gong et al., 2020). The Fe isotope compositions were determined using Nu plasma II multiple collector-inductively coupled plasma-mass spectrometer (MC-ICP-MS). Reference material GSB Fe standard (a substitution of IRMM-014; $\delta^{56}Fe_{IRMM\text{-}014} = \delta^{56}Fe_{GSB} + 0.729$, $\delta^{57}Fe_{IRMM\text{-}014} = \delta^{57}Fe_{GSB} + 1.073$; He et al., 2015) was used for bracketing each sample. Fe isotope compositions are reported as δ-notation relative to the international standard of IRMM-014: $\delta^{i}Fe$ (‰) $= [(^{i}Fe/^{54}Fe)_{sample} \ / \ (^{i}Fe/^{54}Fe)_{IRMM\text{-}014} - 1] \times 1000$, where i refers to mass 56 or 57. Our analyzed $\delta^{56}Fe$ values for USGS standards (W-2a, BCR-2 and BHVO-2) agree well with recommended values in the literature (e.g., He et al., 2015 and references therein; Supplementary Table S1).

For Sr–Nd–Pb–Hf isotopes, about 50 mg of each sample was dissolved in a distilled HNO_3-HCl-HF mixture in a Teflon beaker at 190 °C. Sr and Pb were separated by running through Sr-Spec resin. AG resin was used to separate HFSEs and rare earth elements (REEs). Nd was separated using Ln (Nd) resin, and Hf was separated using Ln (Hf) resin, respectively. The purified Sr, Pb and Hf were diluted in 2% HNO_3, and Nd was diluted in Milli-Q H_2O for analysis with Nu plasma II MC-ICP-MS. ^{203}Tl–^{205}Tl isotopes were used as internal standard to correct for mass-dependent Pb isotope fractionation. The Sr, Nd, Pb and Hf isotope ratios were, respectively, normalized to $^{86}Sr/^{88}Sr = 0.1194$, $^{146}Nd/^{144}Nd = 0.7219$, $^{205}Tl/^{203}Tl = 2.3875$ and $^{179}Hf/^{177}Hf = 0.7325$. Standard averages and reproducibility of standards ($\pm 2\sigma$) over the period of data collection were as follows: NBS-987 $^{87}Sr/^{86}Sr = 0.710277 \pm 0.000006$ ($n = 7$), Jndi-1 Nd $^{143}Nd/^{144}Nd = 0.512106 \pm 0.000003$ ($n = 10$), Alfa Hf $^{176}Hf/^{177}Hf = 0.282194 \pm 0.000004$ ($n = 9$) and NBS-981 $^{208}Pb/^{204}Pb = 36.6818 \pm 0.0006$, $^{207}Pb/^{204}Pb = 15.4790 \pm 0.0002$ and $^{206}Pb/^{204}Pb = 16.9304 \pm 0.0002$ ($n = 7$). Detailed methods for Sr–Nd–Pb–Hf elemental separation and isotope analysis are given by Sun et al. (2019).

3.2. Glass major and trace element analyses

Major and trace elements of samples were analyzed using a Photon Machines Excite 193-nm excimer Ar-F laser system attached to an Agilent 7900 ICP-MS. The samples were analyzed using 85 µm spot size, and 8.49 J/cm^2 energy density at a repetition rate of 6 Hz. Each analysis includes 25 s background acquisition (gas blank) followed by 50 s data acquisition. The raw data were processed using ICPMSDataCal_ver11.0 (Liu et al., 2008). All the analyzed elements in each run were normalized to 100% and calibrated using an ablation yield correction factor (AYCF; Liu et al., 2008) based on analysis of multiple reference materials (NIST SRM 610 and BCR-2G). The analytical precision and accuracy are generally within 5% and below 10% respectively for most analyzed elements, and the analytical details are given in Xiao et al. (2020).

4. Results

The major and trace element analyses and isotope compositions for the NMTB samples are given in Supplementary Tables S1–S3. Pervasive alteration of sample SCAN04AR-045-1 causes the deviation of Sr and Pb isotopes from other samples, so we do not use this sample in the following discussion. The $\delta^{56}Fe$ values of the NMTB samples range from 0.00 ± 0.03‰ to $+0.12 \pm 0.04$‰ (2SD), and show systematic variation with latitude (Fig. 2a). The $\delta^{56}Fe$ varies from MORB-like (Teng et al., 2013) in the south to much lighter towards north. In addition, $^{87}Sr/^{86}Sr$, $^{143}Nd/^{144}Nd$, $^{176}Hf/^{177}Hf$, $^{206}Pb/^{204}Pb$, $^{207}Pb/^{204}Pb$ and $^{208}Pb/^{204}Pb$ also vary with latitude (Fig. 2b–f). The Sr–Nd–Pb isotopes, major and trace element compositions confirm previous studies (e.g., Volpe et al., 1987; Stern et al., 1990; Gribble et al., 1998) that the arc signature (e.g., enriched in LILEs with high $^{87}Sr/^{86}Sr$ and low $^{143}Nd/^{144}Nd$) become progressively stronger from south to north.

5. Discussion

The theory states that heavy Fe isotopes are preferentially partitioned into the phase with higher bond strength (e.g., Dauphas et al., 2014; Sossi and O'Neill, 2017). Ferric iron (Fe^{3+}) is predicted to have heavier Fe isotope (i.e., higher $\delta^{56}Fe$) because the smaller ionic radii and higher valence state of Fe^{3+} results in shorter and stronger bonds (Dauphas et al., 2014). Fe isotopes can fractionate when iron incorporates into different phases, leading to different $\delta^{56}Fe$ between different phases. Unlike incompatible elements and

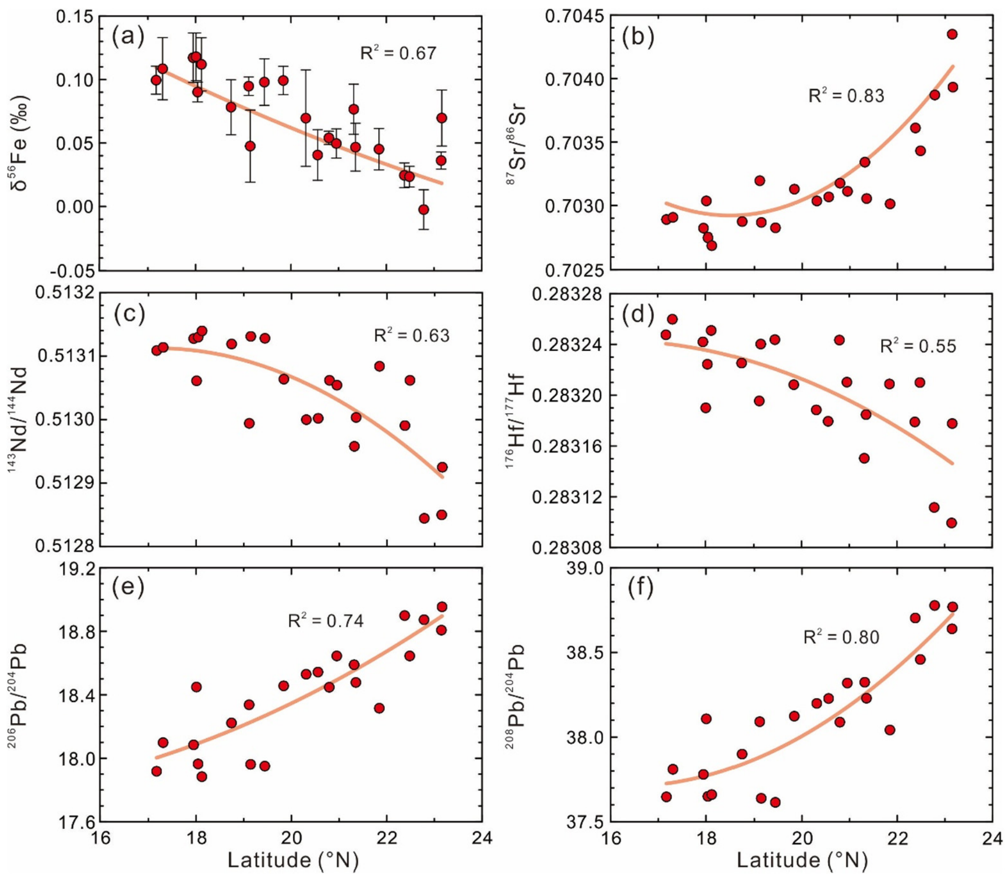

Fig. 2. Systematic variation of δ^{56}Fe (a), ^{87}Sr/^{86}Sr (b), ^{143}Nd/^{144}Nd (c), ^{176}Hf/^{177}Hf (d), ^{206}Pb/^{204}Pb (e) and ^{208}Pb/^{204}Pb (f) with latitude for NMTB. Best-fit lines and R^2 values are given. Error bars in (a) are ± 1SD.

radiogenic isotopes of incompatible elements, only significant mass transfer processes are able to shift Fe isotope composition (Sossi et al., 2016). So, the systematic NMTB Fe isotope variation with latitude must be caused by some major processes which effectively change the Fe isotopes during the magmatism or in the magma source histories. In the following, we use the correlated variations of Fe isotopes (δ^{56}Fe values) with process-sensitive elements and radiogenic isotopes to illustrate and discuss possible factors controlling the variation of Fe isotopes in the context of the NMTB magmatism.

5.1. Effects of fractional crystallization on Fe isotopes

Most of the samples have Mg# > 0.57, and some of them especially the northernmost ones have Mg# as low as 0.38 (Supplementary Table S3). All of these samples have inevitably experienced some extent of fractional crystallization (Supplementary Fig. S1). Previous studies have demonstrated that fractional crystallization of basaltic magmas can cause Fe isotope fractionation (e.g., Sossi et al., 2012; Chen et al., 2021). For a basaltic melt, fractional crystallization of olivine and pyroxene which prefer Fe^{2+} and lighter Fe isotopes will elevate the Fe^{3+} content and δ^{56}Fe value of the residual melt, while fractional crystallization of magnetite which prefer heavier Fe isotopes will decrease the δ^{56}Fe value of the residual melt (e.g., Sossi et al., 2012). Although the high H_2O content in arc magma promotes early crystallization of magnetite (e.g., Feig et al., 2010), the Mariana lava dataset (collected from PetDB) shows that olivine ± clinopyroxene ± plagioclase is the dominant crystallization phases before magnetite crystallization (Supplementary Fig. S1). All of our samples fall into the interval of olivine ± clinopyroxene ± plagioclase crystallization (Supplementary Fig. S1), which indicates that the lower δ^{56}Fe of the NMTB samples towards north are not caused by their more differentiated composition. There are no correlations between δ^{56}Fe and fractionation indices such as MgO or Mg# (Supplementary Fig. S2). In fact, after correcting for the effect of fractional crystallization to Mg# = 0.6 (following Niu and O'Hara, 2008), the corrected data show similar trends with raw data, indicating that the along-axis variation is not caused by magma evolution (Fig. 3). In other words, fractional crystallization is not the cause of the systematic decreasing of δ^{56}Fe of the NMTB samples from south to north (Fig. 2a).

5.2. Influence of partial melting on Fe isotopes

During mantle melting, Fe^{3+} is more incompatible than Fe^{2+} (e.g., Canil et al., 1994), so the melt is expected to have higher $Fe^{3+}/\Sigma Fe$ and δ^{56}Fe than the source and residue although observation evidence is needed. Following the above reasoning, δ^{56}Fe of the melt would increase with decreasing extent of melting for a uniform mantle source (e.g., Williams and Bizimis, 2014; Nebel et al., 2015; Foden et al., 2018). Previous chemical and isotopic studies of lavas from the NMT show that the northernmost rift lavas reflect higher extents of melting than seafloor spreading center lavas in the south (e.g., Stolper and Newman, 1994; Gribble et al., 1998). For our samples, the Na_{60} and Ti_{60} decrease with increasing latitude, which seems to confirm the previous study that the extent of melting increases towards north (Fig. 3a–b). However, with varying sources or source components, any argument for varying extent of melting is unjustified. The systematic variation of Sr–Nd–Pb–Hf isotopes of the NMTB samples with latitude indicates magma source compositional heterogeneity (Fig. 2b–f). The signif-

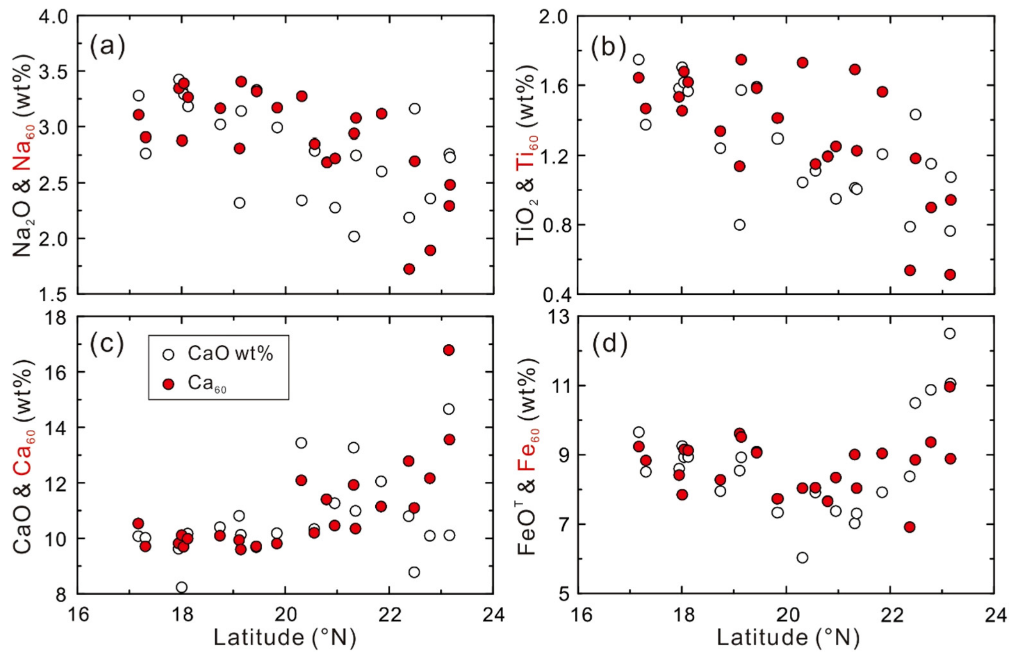

Fig. 3. Plots of Na_{60} (a), Ti_{60} (b), Ca_{60} (c) and Fe_{60} (d) with latitude for the NMTB. The subscript 60 refers to corresponding major element oxides (Na_2O, TiO_2, CaO and FeO^T) corrected for fractionation effect to Mg# = 0.6 following Niu and O'Hara (2008). The uncorrected raw data are plotted for comparison. Both corrected and raw data show similar trends, indicating that the along-axis variation is not caused by magma evolution.

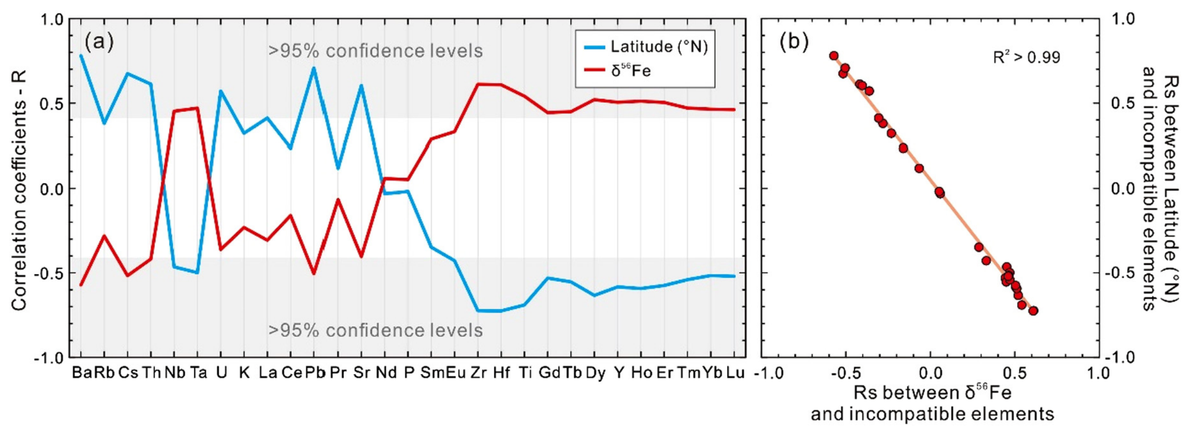

Fig. 4. The composition of NMTB systematically varies with latitude. (a) Correlation coefficients (R-values) diagram of latitude and δ^{56}Fe with incompatible element abundances of NMTB in the order of increasing incompatibility towards left. (b) Elemental correlation coefficients of latitude vs. δ^{56}Fe using data in (a). Fluid-soluble incompatible elements show positive correlation with latitude, but fluid-insoluble incompatible elements (e.g., HREEs and HFSEs) show inverse correlation with latitude. The δ^{56}Fe shows positive correlation with fluid-insoluble (immobile) elements, but inverse correlation with fluid-soluble (mobile) elements, indicating that Fe that hosts ^{56}Fe behaves like an immobile element and has nothing to do with the mobile element characteristics of arc magmatism. The significant correlations of elemental and δ^{56}Fe systematics as a function of latitude indicate that the NMTB record the dynamic processes on the development of a back-arc basin from rear-arc rifting (north) to the mature back-arc spreading center (south).

icant negative correlation of fluid-insoluble elements (e.g., HFSEs and HREEs) and positive correlation of fluid-soluble incompatible elements (e.g., Ba, Cs, Rb, K, Sr, Pb and LREEs) with latitude (Fig. 4a and Supplementary Fig. S3) indicates in simple clarity that these variations do not result from present-day magmatic process, but reflect magma source compositional variation that is consistent with a systematically stronger arc-like geochemical signature towards north. We thus cannot avoid the conclusion that it is the magma source heterogeneity that controls the NMTB Fe isotope variation.

5.3. Source heterogeneity controls on Fe isotope variation in NMTB

As illustrated above, the systematic variations of incompatible element abundances and isotopes with latitude are most consistent with magma source compositional variation (Figs. 2, 4 and Supplementary Fig. S3). From south to north, the variation of Fe isotope and other element or isotope compositions could be caused by varying contributions from (1) asthenosphere, (2) subducting slab, and (3) sub-arc lithospheric mantle (e.g., Volpe et al., 1987; Stern et al., 1990; Gribble et al., 1998; Pearce et al., 2005).

The chemical and isotopic compositions of the samples show that the southernmost samples have the lowest $^{87}Sr/^{86}Sr$ values and the highest δ^{56}Fe, $^{143}Nd/^{144}Nd$ and $^{176}Hf/^{177}Hf$ values (Fig. 2). These characteristics are similar to MORB formed by adiabatic decompression melting of the asthenosphere (Figs. 2, 5 and 6). Previous studies show that the MORB have uniform Fe isotope composition, with an average of about $+0.11 \pm 0.04$‰ (Teng et al., 2013) heavier than their mantle source (δ^{56}Fe = $\sim$+0.02 $\pm$ 0.03‰, Weyer and Ionov, 2007). All this information is consistent with the geological evolution that the southern portion of the NMT (~17–18°N) has already developed into a mature (or almost ma-

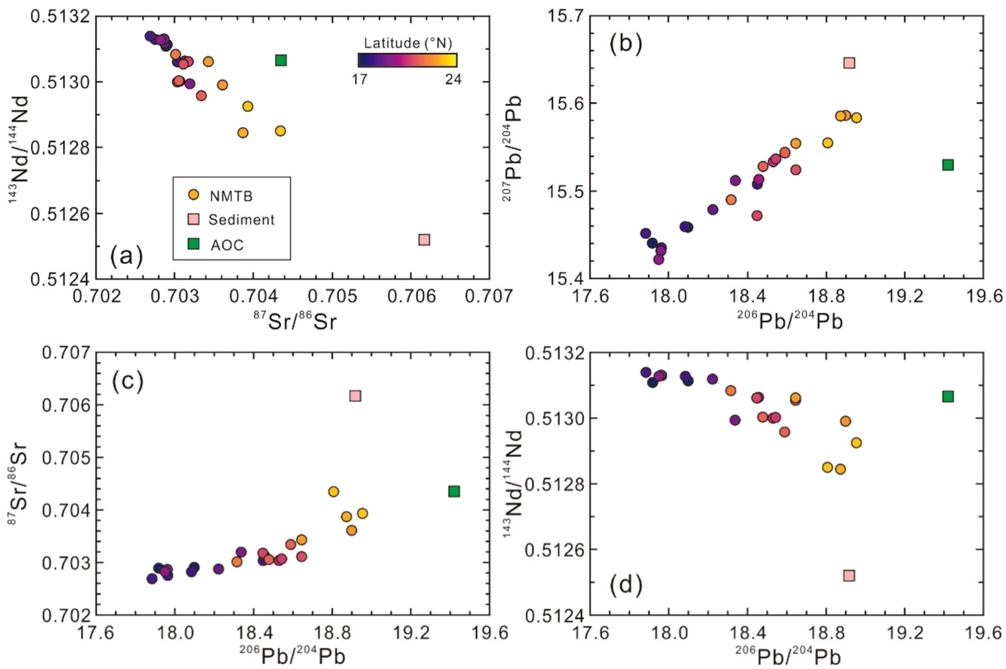

Fig. 5. Sr–Nd–Pb isotope co-variations of the NMTB. (a) $^{87}Sr/^{86}Sr$ vs. $^{143}Nd/^{144}Nd$; (b) $^{206}Pb/^{204}Pb$ vs. $^{207}Pb/^{204}Pb$; (c) $^{206}Pb/^{204}Pb$ vs. $^{87}Sr/^{86}Sr$; (d) $^{206}Pb/^{204}Pb$ vs. $^{143}Nd/^{144}Nd$ for NMTB. Pacific sediment data are from the ODP site 801 (Plank and Langmuir, 1998). Average altered ocean crust (AOC) data are from the ODP site 801 (Hauff et al., 2003). Sr–Nd–Pb isotope systems offer information on magma sources and source histories. Contribution of subducted sediments increases from south to north. (For interpretation of the colors in the figure(s), the reader is referred to the web version of this article.)

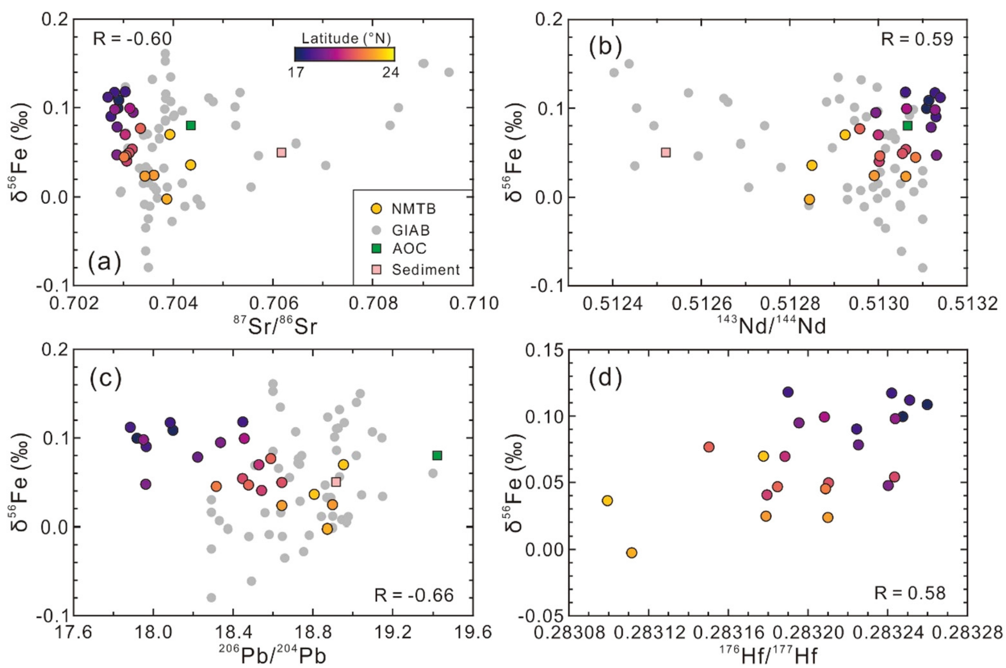

Fig. 6. Variation of $\delta^{56}Fe$ with Sr–Nd–Pb–Hf radiogenic isotopes of the NMTB. Pacific sediment data are from the ODP site 801 (Plank and Langmuir, 1998; Rouxel et al., 2003). Average altered ocean crust (AOC) data are from the ODP site 801 (Hauff et al., 2003; Rouxel et al., 2003). Data of global island arc basalts (GIAB) are from Dauphas et al. (2009), Nebel et al. (2015) and Foden et al. (2018) (using the data with MgO between 4.0–8.5 wt%). The NMTB show correlated variation trends that do not exist in GIAB, the latter indicating contributions of varying slab components to the GIAB $\delta^{56}Fe$, but such slab component, if any, is insignificant in the NMTB.

ture) back-arc spreading center (e.g., Martínez et al., 1995; Gribble et al., 1998; Yamazaki et al., 2003), where the prior mantle lithosphere is essentially gone and the BABB magma source is asthenospheric as indicated by the MORB-like $\delta^{56}Fe$ of $+0.10\text{–}+0.12$‰ (Fig. 2a).

The gradually increasing concentration of fluid-soluble elements towards north (Fig. 4a and Supplementary Fig. S3a–b) indicates the increasing contribution of subducting slab-derived materials (e.g., Volpe et al., 1987; Stern et al., 1990; Gribble et al., 1998; Pearce et al., 2005), while decreasing concentration of fluid-insoluble elements towards north (Fig. 4a and Supplementary Fig. S3c–d) points to the increasing contribution of depleted arc lithospheric mantle resulting from previous melt depletion (Woodhead et al., 1993). In this context, we should note that the nature of such compositionally depleted and physically buoyant sub-arc mantle lithosphere is a straightforward manifestation of subduction initiation as a conse-

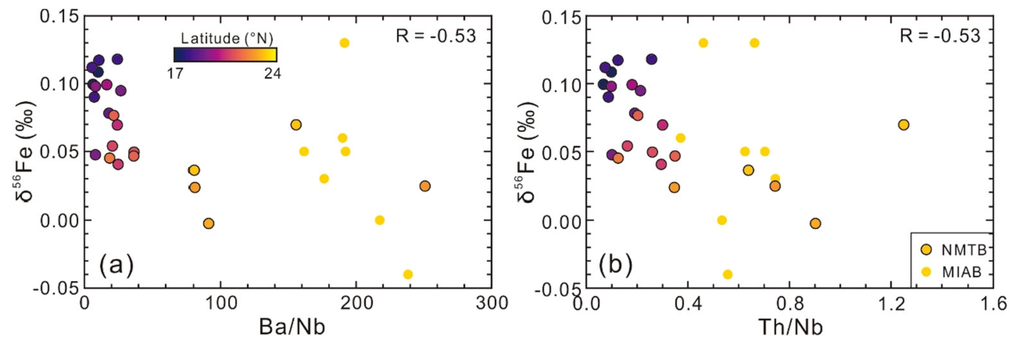

Fig. 7. Plots of δ^{56}Fe against element ratio pairs (Ba/Nb and Th/Nb) of the NMTB. Data of Mariana island arc basalts (MIAB) are from Dauphas et al. (2009) and Williams et al. (2018) (using the data with MgO between 4.0–8.5 wt%). Though the δ^{56}Fe of NMTB shows correlations with arc signature, there is no clear co-variation of δ^{56}Fe with "fluid" or "sediment" tracers for MIAB, suggesting that varying slab components have little contribution to the variation of δ^{56}Fe in the NMTB.

quence of compositional buoyancy contrast within the lithosphere (Niu et al., 2003).

It is important to note that δ^{56}Fe of the NMTB positively correlates with fluid-insoluble elements and negatively correlates with fluid-soluble elements as a function of latitude (Fig. 4a and Supplementary Fig. S3a–b). These correlations can thus be used to discuss magma source compositional contribution (e.g., varying contributions of sub-arc mantle lithosphere vs. slab-derived materials) to δ^{56}Fe of the lavas. To do so, we can first look into δ^{56}Fe of the global arc basalts (using the data with MgO between 4.0–8.5 wt% from Dauphas et al., 2009; Nebel et al., 2015; Foden et al., 2018; Williams et al., 2018) interpreted to reflect varying contributions of slab components.

It is generally assumed that the enrichment in highly incompatible elements of arc magma result from addition of varying combinations of hydrous fluid and silicate melts (partial melts from sediment and altered ocean crust) from subducting slab into the mantle wedge (e.g., Woodhead, 1989; Elliott et al., 1997; Marske et al., 2011). The Sr–Nd–Pb isotope compositions of the samples suggest that the contributions from slab components are dominated by sediment which are increasing from south to north (Fig. 5), which supports the previous interpretation of significant sediment contribution to the northern Mariana arc magmatism (Tollstrup and Gill, 2005). Though previous studies on Fe isotopes of residual slab serpentinites suggest that dehydration of prograde metamorphism of serpentinite can release relatively lighter Fe isotope bearing fluids (δ^{56}Fe < 0.00‰; Debret et al., 2016), there is no clear co-variation of δ^{56}Fe with "fluid" tracers such as Ba/Nb (Fig. 7a; see Williams et al., 2018 for other tracers). The Fe-solubility in hydrous fluid and its contribution to arc magmatism remains under debate (e.g., Nebel et al., 2015; Foden et al., 2018; Castillo, 2021). As for the slab derived melts, there are few studies about the Fe isotope behavior during partial melting of subducting sediments and altered ocean crust. Considering the mineral assemblage of blueschist and eclogite of the subducting ocean crust, we can assume the δ^{56}Fe of slab derived melts is similar to or higher than their protolith. For the Mariana arc, there are no clear correlated variations of δ^{56}Fe with "sediment" tracers such as Th/Nb (Fig. 7b; Williams et al., 2018). For the global arc magmas, the varying contributions of sediment and altered ocean crust give rise to the highly scattered random co-variations of δ^{56}Fe with Sr–Nd–Pb isotopes (Fig. 6a–c). In contrast, the NMTB define correlated variation trends that do not need and cannot be explained by varying slab material contributions (Fig. 6), indicating that the slab component is, if any, insignificant in explaining the NMTB Fe isotope variation. The correlations between δ^{56}Fe and arc signature (such as enriched ^{87}Sr/^{86}Sr, ^{206}Pb/^{204}Pb, fluid-soluble elements, Ba/Nb and Th/Nb) are not a cause-and-effect relationship, but geographic correlations as function of latitude (Fig. 4).

Unlike incompatible elements and radiogenic isotopes of incompatible elements which are likely to be disproportionately affected by contributions from enriched components (Soderman et al., 2020), the Fe isotope composition of the lavas tends to reflect the composition in the magma source (e.g., Williams and Bizimis, 2014; Nebel et al., 2018; Soderman et al., 2020). The higher incompatibility of Fe^{3+} than Fe^{2+} is expected to cause Fe isotope fractionation during mantle melting with the melt having higher Fe^{3+} and heavier Fe isotopes (higher δ^{56}Fe) than the residue. This expectation is confirmed by a recent study on seamount lavas flanking the East Pacific Rise (Sun et al., 2020), which shows clearly that the enriched mantle source component (i.e., high La/Sm, Sm/Yb, Nb/Zr, ^{87}Sr/^{86}Sr; low ^{143}Nd/^{144}Nd and ^{177}Hf/^{176}Hf) of low-degree melt metasomatic origin is characterized by heavy Fe isotopes (high δ^{56}Fe), whereas the depleted mantle component has light Fe isotopes (low δ^{56}Fe). Therefore, the melting residue will necessarily have light Fe isotopes (low δ^{56}Fe). The significantly positive correlation of δ^{56}Fe with fluid-insoluble elements (HFSEs and HREEs; Fig. 4a and Supplementary Fig. S3c–d) indicates that the Fe that hosts ^{56}Fe behaves like an immobile element which is inherited from the mantle sources. The significantly negative correlation of fluid-insoluble elements and latitude (Fig. 4a and Supplementary Fig. S3c–d) indicates the gradual depletion of magma source towards north. Given the understood tectonic evolution of the NMT development (see above), all the geochemical data consistently point to a previously melt-depleted mantle source towards north, which is most consistent with a harzburgitic composition dominated by olivine and orthopyroxene with little clinopyroxene because it is not only depleted in HFSEs (i.e., Nb, Ta, Zr, Hf, Ti), but also HREEs (Fig. 4). Likewise, such depleted mantle source must also be depleted in Fe^{3+} (vs. Fe^{2+}) and heavier Fe isotopes (^{56,57}Fe), giving rise to lighter Fe isotopes (lower δ^{56}Fe) in the basalts towards the north. This further points to the dominance of lithospheric (vs. asthenospheric) magma source towards the north. All these observations and understanding support the notion that sub-arc lithospheric mantle is compositionally refractory (e.g., Woodhead et al., 1993; Parkinson and Pearce, 1998; Niu et al., 2003; Bénard et al., 2017), which imparts the signature of lighter Fe isotope composition of arc magmas (Nebel et al., 2015, 2018; Foden et al., 2018). Here, we can thus suggest that the lowest δ^{56}Fe value (0.00‰) of the samples to represent the basalt formed from partial melting of the sub-arc lithospheric mantle (Fig. 2a), and predict that typical harzburgitic melting residues without later modification should have δ^{56}Fe < 0.00‰.

With all these chemical and isotopic compositions of the NMTB considered, we can conclude that the contribution of arc lithospheric mantle and slab component progressively decreases, while the contributions of asthenosphere increase from north to south (Fig. 8) in response to the initiation and further development of the NMT back-arc spreading center (see below).

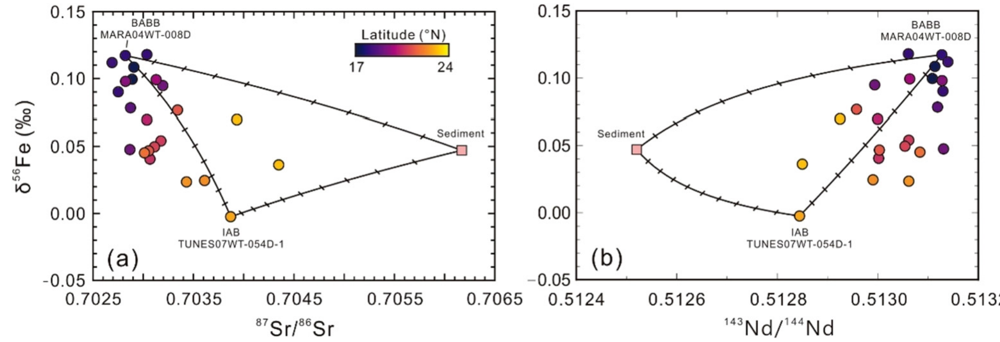

Fig. 8. Source heterogeneity model of δ^{56}Fe and ^{87}Sr/^{86}Sr (a), δ^{56}Fe and ^{143}Nd/^{144}Nd (b). The isotopic composition of the samples result from varying contributions of: (1) asthenosphere (assuming sample MARA04WT-008D as the endmember of BABB inherited from the composition of asthenosphere); (2) sub-arc lithospheric mantle (assuming the sample TUNES07WT-054D-1 as the endmember of IAB inherited from composition of sub-arc lithospheric mantle and inevitable some subducting slab component); (3) sediment (assuming the isotopic composition of sediment for the sediment melt; Plank and Langmuir, 1998; Rouxel et al., 2003). Detailed endmember compositions are given in Supplementary Table S4. The tick marks are interval of 10%.

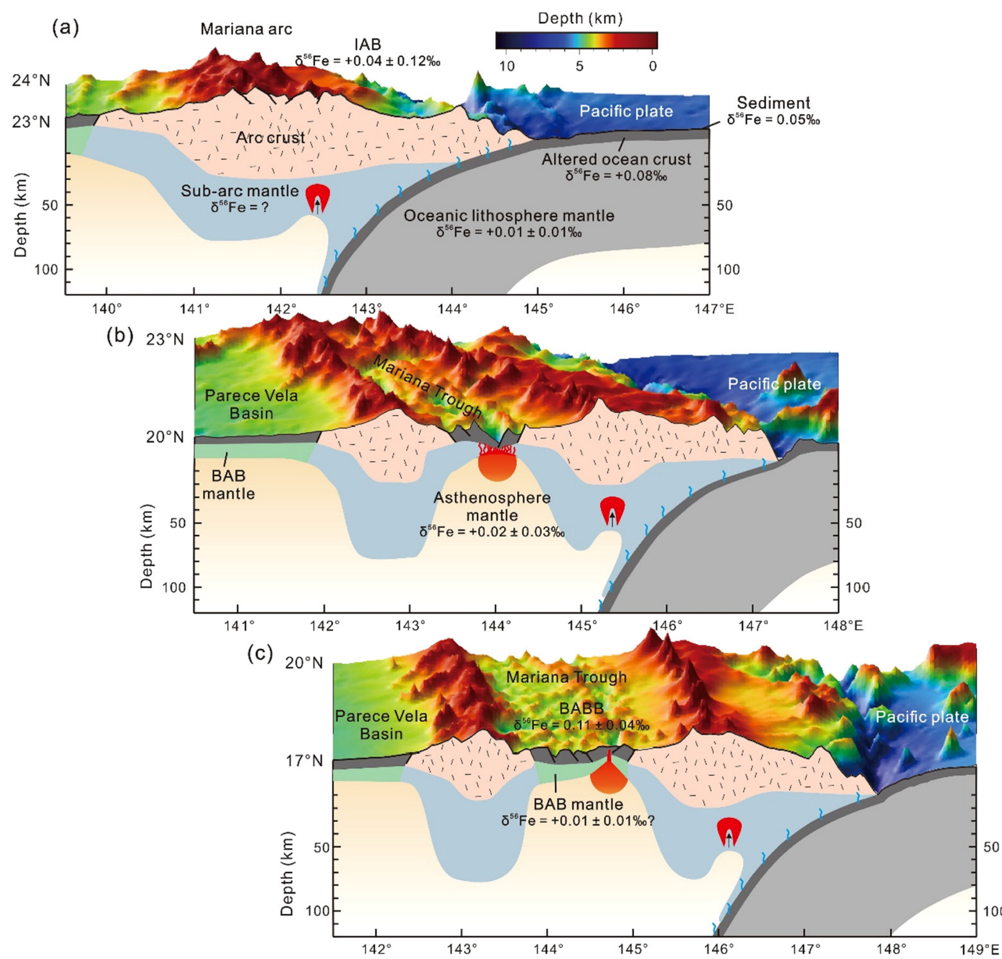

Fig. 9. Schematic illustrations showing Fe isotope variation in varying lithologies in a subduction zone setting such as the Mariana trench-arc-back arc system. The geology of the NMT (17–24°N) furnishes a snapshot of back-arc basin development from rifting in the north to progressively more mature spreading center towards south. From north to south, the previous arc lithospheric mantle (source for IAB) is progressively thinned with the upwelling asthenosphere becomes progressively more important as the source for BABB in mature spreading centers. The variation of δ^{56}Fe as well as other radiogenic isotope compositions of the NMTB are controlled by magma sources with varying contributions of decreasing arc mantle lithosphere and slab components and of increasing asthenosphere from north to south.

5.4. Development of BAB controls BABB magma source heterogeneity

The continued release of hydrous fluid and melts from the subducting Pacific Plate to the lithospheric mantle of the Philippine Sea Plate induce the Mariana arc magmatism (Fig. 9a). The continued seafloor subduction results in trench retreat, overriding plate extension, and the development of back-arc rifting and spreading (Niu, 2014, 2020) (Fig. 9b). The continued extension and back-arc spreading not only thins the prior sub-arc mantle lithosphere, but also facilitates passive asthenosphere upwelling, BABB magmatism and back-arc crustal formation (Fig. 9c). This time sequence of BAB development imparts magma source signatures whose strength decreases in terms of sub-arc lithosphere and slab-derived components and increases in terms of the asthenosphere, which is well characterized by the geology, petrology and geochemistry of the NMT BABB magmatism from north to south. The NMT thus provides a snapshot of the development of a BAB (Fig. 9), which we hypothesize to be of general significance applicable to intra-oceanic BAB development globally.

6. Conclusions

1. The Fe isotope compositions of the NMTB show systematic variation with latitude. The δ^{56}Fe values vary from that similar to the global arc basalts in the north (~0.00‰) to average MORB value in the south (~+0.12‰).
2. This variation cannot be explained by present-day magmatic processes including mantle melting and magma evolution, but is controlled by magma source compositional variation.
3. With incompatible elements and Sr–Nd–Pb–Hf isotopes all considered, the magma source variation resulting from varying contributions of slab-derived component, sub-arc lithospheric mantle and asthenospheric mantle, but the observed δ^{56}Fe variation is predominantly controlled by sub-arc lithospheric mantle and asthenospheric mantle.
4. The arc-like lighter Fe isotope composition to the north is associated with refractory (harzburgitic) sub-arc mantle lithosphere of previous melt depletion at the early stage of rear-arc rifting, whereas the MORB-like Fe isotope composition to the south is dominated by the asthenosphere source in response to the mature and better developed back-arc spreading and asthenospheric mantle upwelling.
5. Sub-arc lithospheric mantle with inherited lighter Fe isotopes is predicted to contribute to the generally lighter Fe isotope composition of arc magmas than MORB. While this prediction is reasonable, we consider it important in future studies to evaluate the potential significance of slab-derived fluids with light Fe isotopes ultimately coming from serpentine dehydration that is largely responsible for flux-melting of arc magmatism.
6. The back-arc spreading center develops from the existing lithosphere whose nature and histories are unknown, but must be compositionally depleted and physically buoyant in terms of major elements and incompatible elements, but the latter could be enriched by subsequent metasomatism without affecting major elements and thus the buoyant nature.
7. The geology and magmatism of the NMT represents a snapshot of the BAB formation and evolution, which we hypothesize to be of general significance that needs testing.

CRediT authorship contribution statement

Yanhong Chen: Data curation, Investigation, Validation, Visualization, Writing – original draft. **Yaoling Niu:** Conceptualization, Methodology, Supervision, Writing – review & editing. **Qiqi Xue:** Investigation. **Yajie Gao:** Investigation. **Paterno Castillo:** Resources, Writing – review & editing.

Declaration of competing interest

The authors declare that they have no known competing financial interests or personal relationships that could have appeared to influence the work reported in this paper.

Acknowledgements

We thank Dr. Yongsheng He for providing the GSB Fe reference material. We thank Editor Rosemary Hickey-Vargas for handling this manuscript and two journal reviewers for constructive comments and suggestions. This study is supported by the National Nature Science Foundation of China (NSFC, Grants No. 91958215 and 41630968), the NSFC-Shandong Joint Fund for Marine Science Research Centers (Grant No. U1606401), and 111 Project (Grant No. B18048).

Appendix A. Supplementary material

Supplementary material related to this article can be found online at https://doi.org/10.1016/j.epsl.2021.117133.

References

Bénard, A., Arculus, R.J., Nebel, O., Ionov, D.A., McAlpine, S.R.B., 2017. Silica-enriched mantle sources of subalkaline picrite-boninite-andesite island arc magmas. Geochim. Cosmochim. Acta 199, 287–303.
Canil, D., O'Neill, H.S.C., Pearson, D.G., Rudnick, R.L., McDonough, W.F., Carswell, D.A., 1994. Ferric iron in peridotites and mantle oxidation states. Earth Planet. Sci. Lett. 123 (1–3), 205–220.
Castillo, P.R., 2021. Chlorine from seawater is key to the generation of calc-alkaline lavas. J. Asian Earth Sci. 213 (15), 104753.
Chen, Y., Niu, Y., Duan, M., Gong, H., Guo, P., 2021. Fractional crystallization causes the iron isotope contrast between mid-ocean ridge basalts and abyssal peridotites. Commun. Earth Environ. 2, 65. https://doi.org/10.1038/s43247-021-00135-5.
Dauphas, N., Craddock, P.R., Asimow, P.D., Bennett, V.C., Nutman, A.P., Ohnenstetter, D., 2009. Iron isotopes may reveal the redox conditions of mantle melting from Archean to present. Earth Planet. Sci. Lett. 288 (1–2), 255–267.
Dauphas, N., Roskosz, M., Alp, E.E., Neuville, D.R., Hu, M.Y., Sio, C.K., Tissot, F.L.H., Zhao, J., Tissandier, L., Médard, C., Cordier, C., 2014. Magma redox and structural controls on iron isotope variations in Earth's mantle and crust. Earth Planet. Sci. Lett. 398, 127–140.
Debret, B., Millet, M.A., Pons, M.L., Bouilhol, P., Inglis, E., Williams, H., 2016. Isotopic evidence for iron mobility during subduction. Geology 44 (3), 215–218.
Deschamps, A., Fujiwara, T., 2003. Asymmetric accretion along the slow-spreading Mariana Ridge. Geochem. Geophys. Geosyst. 4 (10), 8622.
Elliott, T., Plank, T., Zindler, A., White, W., Bourdon, B., 1997. Element transport from slab to volcanic front at the Mariana arc. J. Geophys. Res., Solid Earth 102 (B7), 14991–15019.
Feig, S.T., Koepke, J., Snow, J.E., 2010. Effect of oxygen fugacity and water on phase equilibria of a hydrous tholeiitic basalt. Contrib. Mineral. Petrol. 160 (4), 551–568.
Foden, J., Sossi, P.A., Nebel, O., 2018. Controls on the iron isotopic composition of global arc magmas. Earth Planet. Sci. Lett. 494, 190–201.
Gong, H., Guo, P., Chen, S., Duan, M., Sun, P., Wang, X., Niu, Y., 2020. A re-assessment of nickel-doping method in iron isotope analysis on rock samples using multi-collector inductively coupled plasma mass spectrometry. Acta Geochim. 39 (3), 355–364.
Gribble, R.F., Stern, R.J., Bloomer, S.H., Stüben, D., O'Hearn, T., Newman, S., 1996. MORB mantle and subduction components interact to generate basalts in the southern Mariana trough back-arc basin. Geochim. Cosmochim. Acta 60 (12), 2153–2166.
Gribble, R.F., Stern, R.J., Newman, S., Bloomer, S.H., O'Hearn, T., 1998. Chemical and isotopic composition of lavas from the northern Mariana trough: implications for magmagenesis in back-arc basins. J. Petrol. 39 (1), 125–154.
Hauff, F., Hoernle, K., Schmidt, A., 2003. Sr–Nd–Pb composition of Mesozoic Pacific oceanic crust (site 1149 and 801, ODP Leg 185): Implications for alteration of ocean crust and the input into the Izu-Bonin-Mariana subduction system. Geochem. Geophys. Geosyst. 4 (8), 8913.
Hawkins, J.W., Lonsdale, P.F., Macdougall, J.D., Volpe, A.M., 1990. Petrology of the axial ridge of the Mariana Trough backarc spreading center. Earth Planet. Sci. Lett. 100 (1–3), 226–250.
He, Y., Ke, S., Teng, F.Z., Wang, T., Wu, H., Lu, Y., Li, S., 2015. High-precision iron isotope analysis of geological reference materials by high-resolution MC-ICP-MS. Geostand. Geoanal. Res. 39 (3), 341–356.
Kato, T., Beavan, J., Matsushima, T., Kotake, Y., Camacho, J.T., Nakao, S., 2003. Geodetic evidence of back-arc spreading in the Mariana Trough. Geophys. Res. Lett. 30 (12), 1625.
Liu, Y., Hu, Z., Gao, S., Günther, D., Xu, J., Gao, C., Chen, H., 2008. In situ analysis of major and trace elements of anhydrous minerals by LA-ICP-MS without applying an internal standard. Chem. Geol. 257 (1–2), 34–43.
Marske, J.P., Pietruszka, A.J., Trusdell, F.A., Garcia, M.O., 2011. Geochemistry of southern Pagan Island lavas, Mariana arc: the role of subduction zone processes. Contrib. Mineral. Petrol. 162, 231–252.
Martínez, F., Fryer, P., Baker, N.A., Yamazaki, T., 1995. Evolution of backarc rifting: Mariana Trough, 20–24°N. J. Geophys. Res., Solid Earth 100 (B3), 3807–3827.
Nebel, O., Sossi, P.A., Bénard, A., Wille, M., Vroon, P.Z., Arculus, R.J., 2015. Redox-variability and controls in subduction zones from an iron-isotope perspective. Earth Planet. Sci. Lett. 432, 142–151.
Nebel, O., Sossi, P.A., Foden, J., Bénard, A., Brandl, P.A., Stammeier, J.A., Lupton, J., Richter, M., Arculus, R.J., 2018. Iron isotope variability in ocean floor lavas

and mantle sources in the Lau back-arc basin. Geochim. Cosmochim. Acta 241, 150–163.
Niu, Y.L., 2014. Geological understanding of plate tectonics: basic concepts, illustrations, examples and new perspectives. Glob. Tecton. Metallog. 10, 23–46.
Niu, Y.L., 2020. On the cause of continental breakup: a simple analysis in terms of driving mechanisms of plate tectonics and mantle plumes. J. Asian Earth Sci. 194, 104367.
Niu, Y., O'Hara, M.J., 2008. Global correlations of ocean ridge basalt chemistry with axial depth: a new perspective. J. Petrol. 49 (4), 633–664.
Niu, Y., O'Hara, M.J., Pearce, J.A., 2003. Initiation of subduction zones as a consequence of lateral compositional buoyancy contrast within the lithosphere: a petrological perspective. J. Petrol. 44 (5), 851–866.
Parkinson, I.J., Pearce, J.A., 1998. Peridotites from the Izu–Bonin–Mariana forearc (ODP Leg 125): evidence for mantle melting and melt–mantle interaction in a supra-subduction zone setting. J. Petrol. 39 (9), 1577–1618.
Pearce, J.A., Stern, R.J., Bloomer, S.H., Fryer, P., 2005. Geochemical mapping of the Mariana arc-basin system: implications for the nature and distribution of subduction components. Geochem. Geophys. Geosyst. 6, Q07006.
Plank, T., Langmuir, C.H., 1998. The chemical composition of subducting sediment and its consequences for the crust and mantle. Chem. Geol. 145 (3–4), 325–394.
Rouxel, O., Dobbek, N., Ludden, J., Fouquet, Y., 2003. Iron isotope fractionation during oceanic crust alteration. Chem. Geol. 202 (1–2), 155–182.
Soderman, C.R., Matthews, S., Shorttle, O., Jackson, M.G., Ruttor, S., Nebel, O., Turner, S., Beier, C., Millet, M., Widom, E., Humayun, M., Williams, H.M., 2020. Heavy δ^{57}Fe in ocean island basalts: a non-unique signature of processes and source lithologies in the mantle. Geochim. Cosmochim. Acta 292, 309–332.
Sossi, P.A., Foden, J.D., Halverson, G.P., 2012. Redox-controlled iron isotope fractionation during magmatic differentiation: an example from the Red Hill intrusion, S. Tasmania. Contrib. Mineral. Petrol. 164 (5), 757–772.
Sossi, P.A., Nebel, O., Foden, J., 2016. Iron isotope systematics in planetary reservoirs. Earth Planet. Sci. Lett. 452, 295–308.
Sossi, P.A., O'Neill, H.S.C., 2017. The effect of bonding environment on iron isotope fractionation between minerals at high temperature. Geochim. Cosmochim. Acta 196, 121–143.
Stern, R.J., Lin, P.N., Morris, J.D., Jackson, M.C., Fryer, P., Bloomer, S.H., Ito, E., 1990. Enriched back-arc basin basalts from the northern Mariana Trough: implications for the magmatic evolution of back-arc basins. Earth Planet. Sci. Lett. 100 (1–3), 210–225.
Stolper, E., Newman, S., 1994. The role of water in the petrogenesis of Mariana Trough magmas. Earth Planet. Sci. Lett. 121 (3–4), 293–325.
Sun, P., Niu, Y., Guo, P., Chen, S., Duan, M., Gong, H., Wang, X., Xiao, Y., 2019. Multiple mantle metasomatism beneath the Leizhou Peninsula, South China: evidence from elemental and Sr–Nd–Pb–Hf isotope geochemistry of the late Cenozoic volcanic rocks. Int. Geol. Rev. 61 (14), 1768–1785.
Sun, P., Niu, Y.L., Guo, P.Y., Duan, M., Wang, X.H., Gong, H.M., Xiao, Y.Y., 2020. The lithospheric thickness control on the compositional variation of continental intraplate basalts: a demonstration using the Cenozoic basalts and clinopyroxene megacrysts from eastern China. J. Geophys. Res. 125, e2019JB019315.
Teng, F.Z., Dauphas, N., Huang, S., Marty, B., 2013. Iron isotopic systematics of oceanic basalts. Geochim. Cosmochim. Acta 107, 12–26.
Tollstrup, D.L., Gill, J.B., 2005. Hafnium systematics of the Mariana arc: evidence for sediment melt and residual phases. Geology 33 (9), 737–740.
Volpe, A.M., Macdougall, J.D., Hawkins, J.W., 1987. Mariana trough basalts (MTB): trace element and SrNd isotopic evidence for mixing between MORB-like and arc-like melts. Earth Planet. Sci. Lett. 82 (3–4), 241–254.
Wessel, P., Luis, J.F., Uieda, L., Scharroo, R., Wobbe, F., Smith, W.H.F., Tian, D., 2019. The generic mapping tools version 6. Geochem. Geophys. Geosyst. 20 (11), 5556–5564.
Weyer, S., Ionov, D.A., 2007. Partial melting and melt percolation in the mantle: the message from Fe isotopes. Earth Planet. Sci. Lett. 259 (1–2), 119–133.
Williams, H.M., Bizimis, M., 2014. Iron isotope tracing of mantle heterogeneity within the source regions of oceanic basalts. Earth Planet. Sci. Lett. 404, 396–407.
Williams, H.M., Prytulak, J., Woodhead, J.D., Kelley, K.A., Brounce, M., Plank, T., 2018. Interplay of crystal fractionation, sulfide saturation and oxygen fugacity on the iron isotope composition of arc lavas: an example from the Marianas. Geochim. Cosmochim. Acta 226, 224–243.
Woodhead, J.D., 1989. Geochemistry of the Mariana arc (western Pacific): source composition and processes. Chem. Geol. 76, 1–24.
Woodhead, J., Eggins, S., Gamble, J., 1993. High field strength and transition element systematics in island arc and back-arc basin basalts: evidence for multi-phase melt extraction and a depleted mantle wedge. Earth Planet. Sci. Lett. 114 (4), 491–504.
Xiao, Y., Chen, S., Niu, Y., Wang, X., Xue, Q., Wang, G., Gao, Y., Gong, H., Kong, J., Shao, F., Sun, P., Duan, M., Hong, D., Wang, D., 2020. Mineral compositions of syn-collisional granitoids and their implications for the formation of juvenile continental crust and adakitic magmatism. J. Petrol. 61 (3), egaa038.
Yamazaki, T., Seama, N., Okino, K., Kitada, K., Joshima, M., Oda, H., Naka, J., 2003. Spreading process of the northern Mariana Trough: rifting-spreading transition at 22°N. Geochem. Geophys. Geosyst. 4 (9), 1075.